LAWRENCE
LIVERMORE
NATIONAL
LABORATORY

UCRL-JRNL-217141

A unified electrostatic and cavitation model for first-principles molecular dynamics in solution

D. A. Scherlis, J.-L. Fattebert, F. Gygi, M. Cococcioni, N. Marzari

November 16, 2005

The Journal of Chemical Physics

A unified electrostatic and cavitation model for first-principles molecular dynamics in solution

Damián A. Scherlis[‡], Jean-Luc Fattebert[†], François Gygi[†], Matteo Cococcioni[‡], and Nicola Marzari[‡]

[‡]*Department of Materials Science and Engineering, Massachusetts Institute of Technology, Cambridge MA 02139, and*

[†]*Center for Applied Scientific Computing, Lawrence Livermore National Laboratory, Livermore CA 94551*

(Dated: September 19, 2005)

Abstract

The electrostatic continuum solvent model developed by Fattebert and Gygi is combined with a first-principles formulation of the cavitation energy based on a natural quantum-mechanical definition for the surface of a solute. Despite its simplicity, the cavitation contribution calculated by this approach is found to be in remarkable agreement with that obtained by more complex algorithms relying on a large set of parameters. Our model allows for very efficient Car-Parrinello simulations of finite or extended systems in solution, and demonstrates a level of accuracy as good as that of established quantum-chemistry continuum solvent methods. We apply this approach to the study of tetracyanoethylene dimers in dichloromethane, providing valuable structural and dynamical insights on the dimerization phenomenon.

I. INTRODUCTION

The importance of electronic structure calculations in solution is self-evident: chemistry in nature and in the laboratory often takes place in water or other solvents, or at a solid-solvent interface. This is true for all of biochemistry, for most of organic, inorganic, and analytical chemistry, and for a vast part of materials and surface sciences. The natural solution to this problem is to explicitly include the solvent molecules in the system, either as one or several solvation shells or as a bulk medium that fills the simulation box in periodic boundary conditions. Such approach rapidly increases the expense of the calculation and is not always affordable. The reasons are twofold: the cost of an electronic-structure calculation scales as the cube of the number of atoms considered, at fixed density. Also, one needs to ensure that the solvent is treated appropriately as a liquid medium, using e.g. extensive Monte Carlo or molecular dynamics simulations. Given the large ratio between the number of degrees of freedom in the solvent vs. the solute, the statistical accuracy needed makes most of these approaches prohibitively expensive. The use of hybrid quantum-mechanical/molecular-mechanics (QM/MM) techniques,[1–3] in which the solvent atoms are represented with point (or Gaussian) charges and classical potentials, can sensibly alleviate the cost of the computations, but does not remove the requirement of long dynamical trajectories of the combined quantum and classical fragments to simulate the liquid state of the solvent and to extract thermodynamical averages.

Alternative to these explicit approaches, a description of the solvent as a continuum dielectric medium surrounding a quantum-mechanical solute has long been established, and has proved efficient and accurate in a diversity of cases.[4–7] In continuum schemes the dielectric fills the space outside a cavity where the solute is confined; the shape of this cavity,

considered as a single sphere[8] or ellipsoid in early implementations, has evolved to more realistic molecular shapes such as those defined by interlocking spheres centered on the atoms or by isosurfaces of the electron density.[4,6] In the context of continuum models the interaction between the dielectric medium and the charge distribution of the solute provides the electrostatic part of the solvation free energy, ΔG_{el}, which is the dominant contribution for polar and charged solutes. Solvation effects beyond electrostatic screening, conventionally partitioned in cavitation, dispersion, and repulsion,[6] are also important and will be discussed in the context of our model in Section II. In principle, the application of the continuum model demands that no strong specific interactions are present between the solvent and the solute molecules, although the solvent can always be reintroduced explicitly as an "environmental" skin for the first solvation shells.

Inexpensiveness is not the single asset of continuum models against explicit solvent methods. Unless Monte Carlo or molecular dynamics techniques are used, it is unclear what orientation to choose for the molecules in an explicit solvent model, and even for a medium-sized solute there may be a large number of possible configurations with multiple local minima.[7] More importantly, geometry relaxations will describe a solid or glassy phases for the solvent, with a static dielectric screening that may differ substantially from that of the liquid. This is particularly true for water, where the static permittivity at room temperature is about twenty times larger than that of ice. When geometry optimizations including many solvent molecules are performed, changes in the solute—e.g. the hydration energy—remain "buried" or hidden by the large contributions coming from the energy of the solvent. To extract meaningful information, Monte Carlo or molecular dynamics simulations with accurate thermalizations and averaging times are necessary. Still, it is far from clear that even first-principles molecular dynamics treatments of a solvent would provide the accu-

racy needed to reproduce static screening as a function of temperature (as an example, the dielectric constant of water varies between 87.8 at 0 $^{\circ}C$ and 55.8 at 100 $^{\circ}C$). Room temperature is well below the Debye temperature of many solvents, and thus the effect of quantum, Bose-Einstein statistics can be very important. In fact, recent first-principles molecular dynamics studies of water point to the fact that a combination of inaccuracies in the quantum-mechanical models (such as density-functional theory in generalized-gradient approximations) and the use of Boltzmann statistics produce an overstructured description of water[9−11], with apparent freezing roughly a hundred degrees above the experimental point. Last, the relaxation times needed to extract thermodynamical data from a solvated system can be exceedingly long,[12] compounding many of the issues highlighted here (dynamical, as opposed to static screening, would require to take into account the solvent relaxation times, either explicitly or via a frequency-dependent dielectric model, but such a framework goes beyond the scope of this paper). Continuum solvent methods are free from these issues, and for this reason alone they may be the first choice even when computational resources are not the main constraint.

The presence of a polarizable dielectric will induce a charge redistribution in the solute, which in turn will affect the polarization of the medium. In the self-consistent reaction field approach (SCRF) the dielectric medium and the electronic density respond to the electrostatic field of each other in a self-consistent fashion.[4] Over the past twenty five years a number of developments stemming from the SCRF approach have been proposed and further elaborated.[13−23] Among these, the Polarizable-Continuum Model (PCM) of Tomasi et al.[5,13,19] and the Conductorlike Solvation Model (COSMO) of Klamt and Schüürmann[17] are probably the most-widely used choices in quantum chemistry applications. In both cases the dielectric constant ϵ is taken to be 1 inside the cavity, and a fixed value outside (equal to

the dielectric constant of the solvent for PCM, or infinite for the case of COSMO). The electrostatic problem is then formulated in terms of apparent surface charges (ASC) distributed on the solute-solvent interface. For first-principles molecular dynamics applications, the discontinuity of ϵ at the interface needs to be removed to calculate accurately the analytic derivatives of the potential with respect to the ionic positions. This may be accomplished with the use of a smoothly varying dielectric potential that restores well-behaved analytic gradients.[21] Still, Born-Oppenheimer ab-initio molecular dynamics in localized basis sets are demanding enough that they have yet to be combined, to the best of our knowledge, with the ASC approach for realistic simulations of medium or large system.

On the other hand, first-principles implementations of the continuum solvent model within the Car-Parrinello framework[24] have been devised,[25–28] even though dynamical studies have been reported, to the best of our knowledge, in only few cases.[26,27] In this paper, we introduce a first-principles and conceptually simple approach to the calculation of cavitation energies based on the definition of a quantum surface for the solvent.[54] We combine this scheme with the electrostatic solvation model of Fattebert and Gygi,[26,29], and find a level of accuracy at least as good as that of established quantum-chemistry treatments. The model requires no adjustable parameters other than a universal single-parameter definition of the cavity, and the dielectric constant and the surface tension of the solvent. This combined model is well suited for first-principles molecular dynamics calculations of large finite and extended systems, using e.g. efficient plane-wave Car-Parrinello implementations. In the following sections we describe the method and examine its performance in comparison with experiments and with the well-established PCM approach. Finally, given that cavitation contributions can be particularly important in dimerization processes (where the fusion of two cavities into one provides an additional stabilizing energy), we employ our method to

study the association of the tetracyanoethylene (TCNE) anion in solution[30] by means of static and dynamical simulations, highlighting the role of the cavitation term in the dimerization.

II. THE MODEL AND ITS CONTEXT

A. Preliminary details

Our continuum solvation model has been implemented in the public domain Car-Parrinello parallel code included in the Quantum-ESPRESSO package,[31] based on density-functional theory (DFT), periodic-boundary conditions, plane-wave basis sets, and pseudopotentials to represent the ion-electron interactions. All calculations reported in this work, unless otherwise noted, have been performed using Vanderbilt ultrasoft pseudopotentials,[34] with the Kohn-Sham orbitals and charge density expanded in plane waves up to a kinetic energy cutoff of 25 and 200 Ry respectively. In the Appendix we review the formalism used to calculate energies and forces in periodic boundary conditions in the context of our implementation. Further details can be found in reference [32].

We adopt the definition introduced by Ben-Naim for the solvation free energy,[35] in which ΔG_{sol} corresponds to the process of transferring the solute molecule from a fixed position in the gas phase to a fixed position in the solution at constant temperature, pressure, and chemical composition. For calculation purposes and especially in the case of the continuum dielectric model, ΔG_{sol} can be regarded as the sum of several components, of which the electrostatic, the cavitation, and the dispersion-repulsion contributions are the most relevant ($\Delta G_{sol} = \Delta G_{el} + \Delta G_{cav} + \Delta G_{dis-rep}$).[36] None of these, however, can be directly obtained through experiment, the sum of all of them, ΔG_{sol}, being the only measurable quantity.

In our model, ΔG_{el} and ΔG_{cav} are considered explicitly, while $\Delta G_{dis-rep}$, less relevant for the systems considered here, is largely seized by virtue of the parametrization, as part of the electrostatic term. The dispersion-repulsion energy may be important in the case of hydrophobic and aromatic species, but its explicit calculation is beyond the aim of the present work—in particular, the implementation of the technique proposed by Floris, Tomasi and Pascual Ahuir[37,38] would be straightforward in our model.

B. Electrostatic solvation energy

The electrostatic interaction between the dielectric and the solute is calculated as proposed by Fattebert and Gygi.[26,29] In the following we provide an outline of the model.

The Kohn-Sham energy functional[39] of a system of ions and electrons can be written as

$$E[\rho] = T[\rho] + \int v(\mathbf{r})\rho(\mathbf{r})d\mathbf{r} + E_{xc} + \frac{1}{2}\int \rho(\mathbf{r})\phi[\rho]d\mathbf{r} \tag{1}$$

where the terms on the right hand side correspond to the kinetic energy of the electrons, the interaction energy with the ionic potential, the exchange-correlation energy, and the electrostatic energy E_{es} respectively. In the standard energy functional, the electrostatic potential $\phi[\rho]$ is the solution to the Poisson equation in vacuum,

$$\nabla^2\phi = -4\pi\rho \ . \tag{2}$$

In the presence of a dielectric continuum with a permittivity $\epsilon[\rho]$, the Poisson equation becomes

$$\nabla\cdot(\epsilon[\rho]\nabla\phi) = -4\pi\rho \ . \tag{3}$$

By inserting the charge density obtained from Eq. (3) into the expression for the electrostatic

energy, and integrating by parts, we obtain:

$$E_{es} = \frac{1}{8\pi} \int \epsilon[\rho](\nabla\phi[\rho])^2 d\mathbf{r}. \tag{4}$$

While Eq. (2) can be efficiently solved in reciprocal space with the use of fast Fourier transforms, for arbitrary $\epsilon[\rho]$ the Poisson equation (3) must be solved with an alternative numerical scheme. In the present case, it is discretized on a real space grid, and solved iteratively using a multigrid technique.[26] The functional derivative of E_{es} with respect to ρ yields ϕ and an additional term V_ϵ, originating in the dependence of the dielectric function on the charge density:

$$\frac{\delta E_{es}}{\delta\rho}(\mathbf{r}) = \phi(\mathbf{r}) + V_\epsilon(\mathbf{r}), \tag{5}$$

$$V_\epsilon(\mathbf{r}) = -\frac{1}{8\pi}(\nabla\phi(\mathbf{r}))^2 \frac{\delta\epsilon}{\delta\rho}(\mathbf{r}). \tag{6}$$

The self-consistent Kohn-Sham potential is constructed summing V_ϵ and the electrostatic potential ϕ, to which contributions from the exchange-correlation, and the local and non-local terms in the pseudopotentials are also added (see Appendix). The dielectric medium and the electronic density then respond self-consistently to each other through the dependence of ϵ on ρ and viceversa.

As already mentioned in the introduction, in Gaussian-basis sets implementations of the continuum model ϵ is a binary function with a discontinuity at the cavity surface. The accurate representation of such a function would require unrealistic high kinetic energy cutoffs for the plane wave basis and expensive real space grids. The use of smoothly varying dielectric functions instead eases the numerical load and avoids discontinuities in the forces, essential to proper energy conservation during molecular dynamics simulations. Also, a smooth decay of the permittivity in the proximity of the solute-solvent boundary may even be considered a more physical representation than a sharp discontinuity. In our implementation

the dielectric medium is defined using two parameters ρ_0 and β:

$$\epsilon(\rho(\mathbf{r})) = 1 + \frac{\epsilon_\infty - 1}{2}\left(1 + \frac{1 - (\rho(\mathbf{r})/\rho_0)^{2\beta}}{1 + (\rho(\mathbf{r})/\rho_0)^{2\beta}}\right). \tag{7}$$

This function asymptotically approaches ϵ_∞ (the permittivity of the bulk solvent) in regions of space where the electron density is low, and 1 in those regions where it is high. The parameter ρ_0 is the density threshold determining the cavity size, whereas β modulates the smoothness of the transition from ϵ_∞ to 1.

C. Cavitation energy

The cavitation energy ΔG_{cav} is defined as the work involved in creating the appropriate cavity inside the solution in the absence of solute-solvent interactions.[5] Different approaches have been introduced to compute ΔG_{cav}; nevertheless it is unclear which one is the most accurate given the unavailability of experimental values to compare. Formulations based on the scaled particle theory[40,41] have been originally proposed by Pierotti[42] and further developed in several studies.[43–47] Although these approaches are derived from a rigorous statistical mechanics standpoint, eventually the use of a set of fitted parameters is needed to represent an effective radius for the solvent and for the spheres centered on the solute atoms. For nonspherical cavities, one of the most used approximations is the so-called Pierotti-Claverie formula:[6,43]

$$\Delta G_{cav} = \sum_{k=1}^{N} \frac{A_k}{4\pi R_k^2} G_{cav}(R_k). \tag{8}$$

Eq. (8) describes the cavity as the volume occupied by N interlocked spheres centered on the atoms; A_k is the area of atom k exposed to the solvent, R_k is its van-der-Waals radius, and $G_{cav}(R_k)$ is the cavitation free energy associated to the creation of a spherical cavity of radius R_k according to Pierotti.[42]

Efforts have also been made to describe ΔG_{cav} as a function of the macroscopic surface tension of the solvent γ.[48-50] The suggestion of Uhlig[48] of expressing the work involved in producing the cavity as the product between γ and the area of a sphere, $\Delta G_{cav} = 4\pi R^2\gamma$, has been extended to account for the curvature of the solute-solvent interface, according to the theory of Tolman for the surface tension of a droplet.[51] The validity of simplified expressions of the kind

$$\Delta G_{cav} = PV + 4\pi R^2\tilde{\gamma}\left(1 - \frac{2\delta}{R}\right) \tag{9}$$

has been investigated by different authors[52,53] by means of Monte Carlo simulations with classical potentials. In Eq. (9), $\tilde{\gamma}$ is an effective surface tension for the interface, R is the radius of the cavity, and δ is a coefficient that would correspond to the Tolman length in the case of a macroscopic surface. Studies from both Floris[52] and Chandler[53] groups have shown that $\tilde{\gamma}$ is essentially indistinguishable from the macroscopic surface tension of the solvent, γ. Their simulations have assigned to δ a value of 0.0 in TIP4P water,[52] and of the order of -0.5σ in the case of different Lennard-Jones fluids (σ being the Lennard-Jones radius),[53] suggesting that the curvature correction can in practice be ignored for cavities with radii above only a few Angstroms.

In view of these results, we have chosen to estimate the cavitation energy as the product between the surface tension and the area of the cavity,

$$\Delta G_{cav} = \gamma S(\rho_0), \tag{10}$$

where $S(\rho_0)$ is the surface of the same cavity employed in the electrostatic part of the solvation energy and is defined by an isosurface of the charge density. As observed by Floris et al.,[52] there is always a surface in between the internal and the solvent accessible surfaces such that the correction factor $(1 - \frac{2\delta}{R})$ reduces to 1, entailing a linear dependence between

ΔG_{cav} and the cavity area. We rely on the parametrization of the density threshold ρ_0 to obtain an appropriate surface.

The area of this cavity can be easily and accurately calculated by integration in a real-space grid, as the volume of a thin film delimited between two charge density isosurfaces, divided by the thickness of this film. This idea has been originally proposed by Cococcioni et al.[54] to define a "quantum surface" in the context of extended electronic-enthalpy functionals:

$$S(\rho_0) = \int d\mathbf{r} \left\{ \vartheta_{\rho_0 - \frac{\Delta}{2}} [\rho(\mathbf{r})] - \vartheta_{\rho_0 + \frac{\Delta}{2}} [\rho(\mathbf{r})] \right\} \times \frac{|\nabla \rho(\mathbf{r})|}{\Delta}. \tag{11}$$

The finite-differences parameter Δ determines the separation between two adjacent isosurfaces, one external and one internal, corresponding to density thresholds $\rho_0 - \Delta/2$ and $\rho_0 + \Delta/2$ respectively. The spatial distance between these two cavities—or the thickness of the film—is given at any point in space by the ratio $\Delta/|\nabla\rho|$. The (smoothed) step function ϑ is zero in regions of low electron density and approaches 1 otherwise, and it has been defined consistently with the dielectric function of Eq. (7):

$$\vartheta[\rho(\mathbf{r})] = \frac{1}{2} \left[\frac{(\rho(\mathbf{r})/\rho_0)^{2\beta} - 1}{(\rho(\mathbf{r})/\rho_0)^{2\beta} + 1} + 1 \right]. \tag{12}$$

Note that the volume of the cavity is simply the integral of ϑ on all space:

$$V_c(\rho_0) = \int d\mathbf{r} \; \vartheta_{\rho_0}[\rho(\mathbf{r})]. \tag{13}$$

The functional derivative of $\Delta G_{cav} = \gamma S(\rho)$ with respect to the density gives then the additional contribution to the Kohn-Sham potential,

$$\frac{\delta \Delta G_{cav}}{\delta \rho}(\mathbf{r}) = \frac{\gamma}{\Delta} \times \left[\vartheta_{\rho_0 - \frac{\Delta}{2}} [\rho(\mathbf{r})] - \vartheta_{\rho_0 + \frac{\Delta}{2}} [\rho(\mathbf{r})] \right] \times \left[\sum_i \sum_j \frac{\partial_i \rho(\mathbf{r}) \partial_j \rho(\mathbf{r}) \partial_i \partial_j \rho(\mathbf{r})}{|\nabla \rho(\mathbf{r})|^3} - \sum_i \frac{\partial_i^2 \rho(\mathbf{r})}{|\nabla \rho(\mathbf{r})|} \right] \tag{14}$$

where the indices i and j run over the x, y, z coordinates, and ∂_i indicate a partial derivative with respect to the position.

The exact value of the discretization Δ is not important, as long as it is chosen within certain reasonable limits—a very low value would introduce numerical noise, while a too large one would render an inaccurate measure of the surface. The freedom in the choice of Δ is illustrated in Fig. 1, where the dependence of S on this parameter is examined for a water molecule at various thresholds. For ρ_0 equal or above 0.00048, the calculation of the cavity area is fairly converged for any value of Δ within the range displayed in the figure. We have adopted a value of Δ=0.0002 in our simulations. It is worth noting, on the other hand, that the dependence of the surface on the density threshold ρ_0 is only moderate, reflecting the fact that at the "molecular boundary", the electron density decays significantly on a short distance. This behavior is portrayed in Fig. 1, where it can be seen that for a given Δ, the calculated surfaces change in only about 25% when ρ_0 is increased three times. ΔG_{cav} is in fact much less sensitive to the electron density threshold than ΔG_{el}.

III. RESULTS AND DISCUSSION

A. Solvation energies in water

The only adjustable parameters in our solvation model are ρ_0 and β, which determine the shape of the cavity according to Eqs. (7) and (12). Other parameters entering the model, namely the static dielectric constant and the surface tension of the solvent, are physical constants taken from experiments. We have actually kept ρ_0 as the single degree of freedom to fit the solvation energy, while fixing the value of β to 1.3 as in reference [29]. This choice of β provides a smooth, numerically convenient transition for the step function, still ensuring that the lower and upper limits of $\epsilon(\rho(\mathbf{r}))$ and $\vartheta(\rho(\mathbf{r}))$ are reached reasonably fast. The parameter ρ_0 was obtained from a linear least squares fit to the hydration energies of three

solutes: amide, nitrate, and methylammonium (a polar molecule, and two ions of opposite sign). The resulting value, ρ_0 =0.00078, was employed thereafter in all the simulations. This can be regarded as a rather universal choice for ρ_0 and β; reparametrizations for different solvents could be considered (if enough experimental data were available) probably gaining some marginal accuracy at the expense of generality.

Table I shows the solvation and cavitation energies in water calculated for a number of neutral species, along with their experimental values.[55–57] A quite remarkable agreement with experiments is found. We compare the data with PCM results obtained at the DFT-PBE/6-311G(d,p) level (or DFT-PBE/3-21G** for the case of Ag^+) using the Gaussian 03 package.[58] Also significant is the accord between the cavitation energies computed with the two methods—with the caveat that in Gaussian-PCM ΔG_{cav} is based on the Pierotti-Claverie formula (see Eq. (8)) which requires a lengthy list of parameters including all van-der-Waals radii. Similar agreement between the values of ΔG_{cav} coming our approach and PCM is found among charged solutes as shown in Table II. The level of accuracy in ΔG_{sol} is in this case as good as for the neutral solutes, if viewed in relative terms (we point out that, regarding the experimental values of ΔG_{sol} reported for ions, discrepancies between sources up to a few kcal/mol are common).

The solvation energies of the ionic solutes showed in Table II were calculated including the Makov-Payne correction,[59] which takes into account how the gas phase energy of a charged system is affected by its periodic images in supercell calculations:

$$E_{GAS} = E_{PBC} + \frac{q^2\alpha}{2L} - \frac{2\pi qQ}{3L^3} + O[L^{-5}], \tag{15}$$

where E_{GAS} and E_{PBC} are the isolated and the supercell energies respectively, q is the charge of the system, Q its quadrupole moment, L the lattice parameter, and α the Madelung constant (we used a simple cubic lattice of charges, for which α=2.8373[60]). As shown in

Fig. 2 for the nitrate anion, the dependence of the energy with respect to the inverse of the lattice parameter becomes virtually linear for L above 40 a.u., pointing out that the quadrupole term can be neglected in supercells of that size or larger. So, we applied the Makov-Payne correction to the $1/L$ leading order to all the cations and anions in Table II, always checking for convergence with respect to $1/L$. The gas phase energies calculated in this way were subtracted from the correspondent energies in solution to obtain ΔG_{sol}. Fig. 2 also shows that total energies in solution quickly converge with respect to the size of the supercell, thanks to the dielectric screening of the Coulombic interactions between periodic images.

With the exception of CH_4, the solutes in Tables I and II are either polar or ionic compounds of relatively small size. Since the dispersion-repulsion energy is not explicitly accounted for in our model, its accuracy for systems in which this contribution becomes dominant, such as highly hydrophobic or aromatic compounds, will be necessarily affected (this is already the case for methane). For the species listed in Tables I and II the dispersion-repulsion effect is captured to a large extent by our electrostatic term. As the size of the solute increases and its polarity decreases, though, the non-electrostatic terms tend to monopolize the solvation energy, and a model lacking the dispersion-repulsion contribution will perform poorly. This limitation could be possibly overcome by a different parametrization specific to large nonpolar solutes, or of course by directly computing the dispersion and repulsion contributions.[37,38]

B. Molecular dynamics and total energy conservation

As a computational test, we performed canonical molecular dynamics simulations of a tetramer of D_2O molecules (heavy water), using our solvation-cavitation model to represent

an aqueous solution. A time step of 0.192 fs and an electronic mass of 400 a.u. were employed, and the system was thermalized at 350 K by applying the Nose-Hoover thermostat on the ions. Fig. 3 shows the initial configuration of the cluster, where the four D_2O molecules are stabilized in a ring by four hydrogen bonds. In the upper part of Fig. 4, the total energy is monitored throughout the run and compared with the potential energy. The conservation of the total energy is as good as in the gas phase for the same simulation parameters, and is not affected by the dissociation of the bonds. The analysis was not pursued beyond 0.65 ps, when the water cluster dissolves into the medium and one of the D_2O molecules evolves close to the border of the real space grid, affecting the Dirichlet boundary conditions.

In the lower section of Fig. 4, the intermolecular O$\cdots$H distance is plotted for the four initial hydrogen bonds that keep the cluster bound. The solvent dissociates this structure early in the simulation, and before half a picosecond only one hydrogen bond has survived. By the end of the run a dimer is what remains of the original tetramer. For comparison, long molecular dynamics (up to 10 ps) were carried on in the gas phase under identical conditions. In this case the cyclic cluster is stable for the full length of the simulation, showing that the disruption of the intermolecular bonds is indeed a consequence of the solvation effect.

C. Dimerization of TCNE anions in solution

Starting in the early 60's, dimerization of charged and neutral organic π radicals in solution and in the solid state was reported by several authors.[61–67] The discovery of this phenomenon prompted a vast amount of research which has continued up to the present day.[30,68–72] Among the systems addressed, significant efforts have gone into the study of the tetracyanoethylene anion $[TCNE]^{-\cdot}$ and its salts because of their central role in the understanding and development of molecular metals. Recently, evidence has been presented

showing that the dimerization of $[TCNE]^{-\cdot}$ in the solid state involves two-electron four-center π^*–π^* bonding arising from the interaction of the two singly occupied molecular orbitals (SOMOs) of the anions and leading to long (≈ 3.0 $\AA$) intermonomer C–C covalent bonds.[68,69] Data from UV-vis and EPR spectroscopies suggested the same conclusions are true in the solvated state.[30,69] In the gas phase, DFT and MP3 calculations show that the dimer is only metastable, since the attractive covalent interaction between the anions is outweighed by the Coulombic repulsion.[68,69,72] In the solid state, in contrast, the positive counterions stabilize the array of like charges, allowing the π^*–π^* bonding to occur.[68,69]

A solvent may play an analogous role in stabilizing the dimer, by favoring the concentration of charge in a single cavity. We used our solvation model to fully optimize the doubly charged TCNE dimer[73] in dichloromethane, properly adapting the values of ϵ and γ (8.93 a.u. and 27.20 mN/m respectively). We found a stable minimum at an equilibrium distance of 3.04 $\AA$, in close agreement with solid state geometries: X-ray data of different salts[74–76] range from 2.83 to 3.09 $\AA$. The CN substituents deviate from the plane by 5° (see Fig. 5), consistently with the NC-C-C-CN dihedral angles observed in crystals, between 3.6 and 6.5°. This deviation has been ascribed to the rehybridization of the sp^2 carbon as the intradimer bond is formed,[68] but its origin could be also tracked to the steric repulsion between the CN moieties facing each other.

Fig. 6 (upper panel) shows the binding energy for the $[TCNE]_2^{2-}$ in dichloromethane as a function of the separation between the $[TCNE]^{-\cdot}$ fragments. At every point, all coordinates were relaxed while freezing the intradimer distance. The curve presents a steep minimum at 3.04 $\AA$, with a barrier to dissociation of nearly 4 kcal/mol. The grouping of two monomers inside a single cavity, of an area smaller than the one corresponding to two separate cavities containing one monomer each, is energetically favored by the surface tension of the solvent.

Thus, if the contribution of the cavitation energy to the solvation is not considered, the binding results weaker, as seen in Fig. 6. The surface of the cavity, plotted in the lower panel, increases gradually as the monomers are pulled apart, until the solvation cavity splits in two at around 5 $\mathring{A}$. (this is a case in which different β in the parametrization could account for the distinctive ability of solvents to penetrate narrow spaces). Beyond this point the total surface remains constant as each $[TCNE]^{-\cdot}$ unit occupies a separate cavity, and the two curves in the top panel merge. The ground state of the system is a singlet for distances up to 4.0 $\mathring{A}$, whereas at larger separations the spins of the fragments are no longer paired, conforming to a triplet state.

A value of -1.1 kcal/mol is obtained for the binding energy between the monomers. Such a value is underestimated with respect to the experimental dimerization enthalpy, ΔH_D, reported in the range of -6.9 – -9.8 kcal/mol in dichloromethane.[30] The disagreement can be partially attributed to the inability of DFT to fully account for the correlation energy involved in the π^*–π^* bond, and also, to some extent, to the effect of the counterions present in the solution, which differentially stabilize $[TCNE]_2^{2-}$ compared to two $[TCNE]^{-\cdot}$ anions. This effect has been advocated in a recent study[72] of the interaction of two $[TCNE]^{-\cdot}$ fragments in tetrahydrofuran (ϵ=7.58) using PCM at the MP2 level, to explain why the dimer was found metastable by 9.7 kcal/mol with respect to the isolated monomers—the experimental estimate for ΔH_D being -8 kcal/mol in 2-methyl-tetrahydrofuran.[65] The binding energy curve presented in that work exhibited a broad minimum extending from 3.1 to 3.7 $\mathring{A}$, a separation range substantially larger than the one observed in the solid state. Our own PCM calculations in dichloromethane, using PBE in combination with the 6-311+G(d,p) Gaussian basis set, yield a metastable dimer with an interaction energy of 3.2 kcal/mol and an equilibrium distance of 3.00 $\mathring{A}$.

Temperature dependence investigations in solution indicate that the dissociated $[TCNE]^{-\cdot}$ anions are the predominant species at ambient conditions, and that the concentration of the dimer rapidly grows as the temperature goes down.[30,69] Car-Parrinello molecular dynamics simulations of the $[TCNE]_2^{2-}$ dimer were performed in dichloromethane at 250 K, with the temperature controlled by the Nose-Hoover thermostat on the ions. A time step of 0.288 fs and an electronic mass of 400 a.u. were used. In Fig. 7, we monitor the evolution of two structural parameters which serve as descriptors of the $[TCNE]^{-\cdot}$– $[TCNE]^{-\cdot}$ bonding. The intradimer separation, departing from a value of 3.9 $\mathring{A}$ corresponding to an initially elongated dimer, drops to nearly 2.7 $\mathring{A}$ and then describes large oscillations in the order of 1 $\mathring{A}$ around the equilibrium distance. The second parameter, corresponding to the C=C$\cdots$C=C dihedral angle formed by the two $[TCNE]^{-\cdot}$ anions, provides a measure of the alignment between the monomers: if this angle is zero the anions lay parallel. Fig. 7 shows that this is not the case most of the time. Rapid oscillations of an average amplitude of 6° take place around the equilibrium angle. During most of the second part of the run the oscillations are not necessarily centered around zero, which is indicative of the relatively lax nature of the bond.

The length of the simulation is enough to reveal some distinctive features of the frequency spectrum of the system in the IR region. The continuous line in Fig. 8 shows the Fourier transform of the velocity-velocity correlation functions corresponding to two pairs of atoms in the dimer. The first pair consists of the two carbon atoms involved in the C=C bond. The autocorrelation function of the relative velocity between these two centers originates an intense peak corresponding to the C=C stretching at 1250 cm^{-1}. The same mode resolved in the case of the monomer (dashed line) shows up at 1310 cm^{-1}. In the solid state, experimental C=C stretching frequencies of 1364 and 1421 cm^{-1} have been reported for the dimer and the monomer respectively.[69] Such discrepancies between our results and the experimental

numbers are expected, given the distinct conditions in the solid and liquid environments, the difference in the temperatures at which the spectroscopic and the computational data were collected, the use of DFT, and the slight downshift in ionic frequencies in Car-Parrinello dynamics.[77] However, we note that the shift of 60 cm^{-1} in going from the monomer to the dimer is nicely reproduced by our simulations.

In an attempt to characterize the frequency of the intradimer π^*–π^* bonding, we have also analyzed the relative-velocity autocorrelation function for the two carbon atoms forming the bond, one atom pertaining to each monomer. The frequency spectrum of this function yields the four groups of signals appearing below 600 cm^{-1} in Fig. 8, the assignment of which is less evident than in the case of the C=C stretching. Although we are unable to unambiguously identify all these frequencies, Fourier transform analysis of the autocorrelation function for the velocity of the center of mass of the two fragments (data not shown) points to the lowest frequency emerging in the spectrum, at 65 cm^{-1}, as the one related to the intradimer vibration. To the best of our knowledge, no experimental data is available for this mode. Interestingly enough, though, the aforementioned theoretical study based on PCM and MP2,[72] predicted an inter-fragment vibrational frequency of 60 cm^{-1} by solving the one-dimensional Scrödinger equation on the potential energy surface calculated for the interaction between the $[TCNE]^{-\cdot}$ anions.

IV. FINAL REMARKS

The electrostatic-cavitation model described in this work enables Car-Parrinello molecular dynamics simulations in a continuum solvent for large finite systems, and shows a level of accuracy as good as that offered by state-of-the-art quantum chemistry solvation schemes. Additionally, our model is suited for the treatment of periodic systems in solution, represent-

ing a powerful tool for the study of solid-liquid interfaces, solvated polymers, and in general extended systems in contact with a solution. Further improvements will be the subject of future work, especially the incorporation of the dispersion-repulsion effects, which become increasingly important with the size of the solute. The method of references [37] and [38] is an attractive choice, although other possible approaches derived from first-principles and employing a minimal number of parameters are also envisioned.

Our cavitation energy, defined in a simple and physical way, can be straightforwardly implemented in plane-waves or real space codes. Interestingly, such definition turned out to be in remarkable agreement with the values provided by more complex algorithms reliant on large sets of parameters.

The real time study of the pairing of $[TCNE]^{-\cdot}$ constitutes the first dynamical ab-initio investigation of dimerization phenomena in solution, of which the formation of the $[TCNE]_2^{2-}$ is just one example. The binding of charged radicals in solution is relevant to a broad field of research in organic and materials chemistry, and proper consideration of the cavitation contribution turns out to be a central ingredient for an accurate atomistic description.

V. ACKNOWLEDGMENTS

The authors thank Patrick Sit for his help in post-processing the velocity autocorrelation functions, and for useful discussions. This research was supported by the MURI Grant DAAD 19-03-1-0169, and by the Institute of Soldier Nanotechnologies, contract DAAD-19-02-D0002, with the U.S. Army Research Office.

This work was performed under the auspices of the U.S. Department of Energy by University of California, Lawrence Livermore National Laboratory under contract W-7405-Eng-48.

VI. APPENDIX

Leaving aside the exchange-correlation energy and the non-local term of the pseudopotential, the electrostatic problem in a system of pseudo-ions (nuclei plus core electrons) and valence electrons may be written[32]

$$E = \sum_{I<J} \frac{Z_I Z_J}{R_{IJ}} + \sum_I \int \rho_e(r) v_{loc}(r - R_I) dr + \frac{1}{2} \int \frac{\rho_e(r)\rho_e(r')}{|r - r'|} dr dr' \tag{16}$$

The first term on the right in Eq. (16) accounts for repulsion between pseudo-ions, the second is the interaction between these ions and the valence electron density, and the third is the Coulombic integral between valence electrons. Let $\rho_I(r - R_I)$ be a Gaussian distribution of negative sign that integrates to the total charge of the pseudo-ion (note that the electronic charge is defined here as positive). Adding and subtracting $\sum_I \rho_I(r - R_I)$ from $\rho_e(r)$ in the third term we obtain

$$\begin{aligned} E = \frac{1}{2} \int [\rho_e(r) + \sum_I \rho_I(r - R_I)][\rho_e(r') + \sum_I \rho_I(r' - R_I)] \frac{1}{|r - r'|} dr dr' \\ - \int \rho_e(r) [\sum_I \rho_I(r' - R_I)] \frac{1}{|r - r'|} dr dr' - \frac{1}{2} \sum_{IJ} \int \rho_I(r - R_I)\rho_J(r' - R_J) \frac{1}{|r - r'|} dr dr' \\ + \sum_I \int \rho_e(r) v_{loc}(r - R_I) dr + \sum_{I<J} \frac{Z_I Z_J}{R_{IJ}} \end{aligned} \tag{17}$$

The first term on the right is the Hartree energy E_H of a pseudopotential code. Introducing the following definitions:

$$E_H = \frac{1}{2} \int [\rho_e(r) + \sum_I \rho_I(r - R_I)][\rho_e(r') + \sum_I \rho_I(r' - R_I)] \frac{1}{|r - r'|} dr dr'$$

$$E_{ps} = \sum_I \int \rho_e(r)[v_{loc}(r - R_I) + v_I(r - R_I)] dr, \quad with\ v_I(r) = -\int \frac{\rho_I(r')}{|r - r'|} dr'$$

$$E_{sr} = -\sum_{I<J} \int \rho_I(r - R_I)\rho_J(r' - R_J) \frac{1}{|r - r'|} dr dr' + \sum_{I<J} \frac{Z_I Z_J}{R_{IJ}}$$

$$E_{self} = -\frac{1}{2} \sum_I \int \rho_I(r - R_I)\rho_I(r' - R_I) \frac{1}{|r - r'|} dr dr'$$

it is possible to write the total energy as:

$$E = E_H + E_{ps} + E_{sr} + E_{self} \tag{18}$$

The pseudo-ions density ρ_I is defined as:

$$\rho_I(r - R_I) = -\frac{Z_I}{(R_I^c)^3}\pi^{-\frac{3}{2}} \exp\left(-\frac{|r - R_I|^2}{(R_I^c)^2}\right) \tag{19}$$

where R_I^c determines the width of the Gaussian associated with the site I. Under such definition E_{self} and E_{sr} can be evaluated analytically. In particular, E_{self} is a constant not dependent on the atomic positions:

$$E_{self} = -\frac{1}{\sqrt{2\pi}} \sum_I \frac{Z_I^2}{R_I^c} \tag{20}$$

$$E_{sr} = \sum_{I<J} \frac{Z_I Z_J}{R_{IJ}} erfc\left(\frac{R_{IJ}}{\sqrt{(R_I^c)^2 + (R_J^c)^2}}\right) \tag{21}$$

The remaining pseudopotential term E_{ps} is computed in reciprocal space, after constructing the pseudopotential v_{loc}^I carrying both contributions from the local pseudopotential v_{loc} and the smeared core charges potential v_I.

$$E_{ps} = \sum_I \int \rho_e(r) v_{loc}^I(r) dr \tag{22}$$

$$v_{loc}^I(r) = v_{loc}(r) + v_I(r) = v_{loc}(r) - \int \frac{\rho_I(r')}{|r - r'|} dr' = v_{loc}(r) - \frac{Z_I}{r} erf\left(\frac{r}{R_I^c}\right) \tag{23}$$

The ionic forces can be obtained from the energies above (plus the non-local pseudopotential term, which will be omitted for simplicity). The Hellmann-Feynman theorem—i.e. the stationariety of the total energy with respect to ψ—gives

$$F_I = -\frac{dE}{dR_I} = -\frac{\partial E}{\partial R_I} - \sum_j \frac{\delta E}{\delta |\psi_j\rangle} \frac{\delta |\psi_j\rangle}{\partial R_I} = \frac{\partial E}{\partial R_I} \tag{24}$$

(real wavefunctions are assumed). Thus,

$$-\frac{dE}{dR_I} = -\frac{\partial E}{\partial R_I} = -\frac{\partial E_H}{\partial R_I} - \frac{\partial E_{ps}}{\partial R_I} - \frac{\partial E_{sr}}{\partial R_I} - \frac{\partial E_{self}}{\partial R_I} \tag{25}$$

Note that the partial derivatives of the individual terms in the Hamiltonian do not correspond to the total derivatives. For example:

$$\frac{\partial E_H(R_1, R_2, ..., R_n)}{\partial R_n} \neq \frac{dE}{dR_I} = \lim_{\epsilon \to 0} \frac{E_H(R_1, R_2, ..., R_n + \epsilon) - E_H(R_1, R_2, ..., R_n - \epsilon)}{2\epsilon}$$

E_{self} does not depend on R_I and therefore does not contribute to the forces, whereas the derivative for E_{sr} can be obtained analytically.

The derivative of E_{ps} results

$$\frac{\partial E_{ps}}{\partial R_I} = \sum_I \int \rho_e(r) \frac{\partial v_{loc}^I(r)}{\partial R_I} dr \tag{26}$$

where the term $\partial v_{loc}^I(r)/\partial R_I$ is straightforward in the reciprocal space:

$$v_{loc}^I(r - R_I) = \sum_{\mathbf{G}} \tilde{v}_G e^{i\mathbf{G}\mathbf{r}} e^{-i\mathbf{G}\mathbf{R_I}}$$

$$\frac{\partial}{\partial R_I} v_{loc}^I(r - R_I) = \sum_{\mathbf{G}} -i\mathbf{G}\tilde{v}_G e^{i\mathbf{G}\mathbf{r}} e^{-i\mathbf{G}\mathbf{R_I}} \tag{27}$$

with $\tilde{v}_G$ the coefficients of the Fourier expansion for $v_{loc}^I(r)$.

Finally, to obtain the contribution from E_H, the Hartree energy is recasted as:

$$E_H = \frac{1}{2} \int \left[\rho_e(r)\rho_e(r') + \sum_I \rho_I(r - R_I) \sum_I \rho_I(r' - R_I) + 2\rho_e(r) \sum_I \rho_I(r' - R_I) \right] \frac{1}{|r - r'|} dr dr'$$

whose derivative with respect to the atomic positions is:

$$\frac{1}{2} \int \left[2 \sum_I \rho_I(r - R_I) \Big(\frac{\partial}{\partial R_I} \sum_I \rho_I(r' - R_I) \Big) + 2\rho_e(r) \Big(\frac{\partial}{\partial R_I} \sum_I \rho_I(r' - R_I) \Big) \right] \frac{1}{|r - r'|} dr dr'$$

$$= \int \Big(\frac{\partial}{\partial R_I} \sum_I \rho_I(r' - R_I) \Big) \Big(\rho_e(r) + \sum_I \rho_I(r - R_I) \Big) \frac{1}{|r - r'|} dr dr'$$

Hence, if $\rho_{tot}(r) = \rho_e(r) + \sum_I \rho_I(r - R_I)$, the contribution from E_H turns out to be

$$\frac{\partial E_H}{\partial R_I} = \int \frac{\rho_{tot}(r)}{|r - r'|} \Big(\frac{\partial}{\partial R_I} \sum_I \rho_I(r' - R_I) \Big) dr dr' \tag{28}$$

where the term $\partial \sum_I \rho_I(r' - R_I)/\partial R_I$ is obtained derivating in the Fourier space in the same fashion as in Eq. (27). The ratio $\rho_{tot}(r)/|r - r'|$ is the Hartree potential V_H, which can be computed in the reciprocal space from the expansion for $\rho_{tot}(r)$.

$$\rho_{tot}(r) = \sum_{\mathbf{G}} \tilde{\rho}_G e^{i\mathbf{G}\mathbf{r}}, \qquad V_H = \sum_{\mathbf{G}} \tilde{\beta}_G e^{i\mathbf{G}\mathbf{r}}$$

$$\nabla^2 V_H = -4\pi\rho_{tot} \Rightarrow \tilde{\beta}_G = -\frac{4\pi}{\mathbf{G}^2}\tilde{\rho}_G$$

$$V_H = \sum_{\mathbf{G}} \frac{-4\pi}{\mathbf{G}^2}\tilde{\rho}_G e^{i\mathbf{G}\mathbf{r}} \tag{29}$$

In the case of the continuum solvent implementation, V_H is replaced by $\frac{\delta E_{es}}{\delta \rho}(\mathbf{r})$ according to Eq. (5) and (6) of the main text.

[1] G. M. Monard and K. M. Merz, Jr, Acc. Chem. Res. **32**, 904 (1999)

[2] M. Eichinger, P. Tavan, J. Hutter, and M. Parrinello, J. Chem. Phys. **110**, 10452 (1999).

[3] A. Crespo, D. A. Scherlis, M. A. Martí, P. Ordejón, A. E. Roitberg, and D. A. Estrin, J. Phys. Chem. B **107**, 13728 (2003).

[4] I. N. Levine, *Quantum Chemistry* (Prentice Hall, New Jersey, 2000).

[5] J. Tomasi and M. Persico, Chem. Rev. **94**, 2027 (1994).

[6] J. Tomasi, B. Mennucci, and R. Cammi, Chem. Rev. **105**, 2999 (2005).

[7] C. J. Cramer and D. G. Truhlar, Chem. Rev. **99**, 2161 (1999).

[8] L. Onsager, J. Am. Chem. Soc. **58**, 1486 (1936).

[9] P. H.-L. Sit and N. Marzari, J. Chem. Phys. **122**, 204510 (2005).

[10] J. C. Grossman, E. Schwegler, E. W. Draeger, F Gygi, and G. Galli, J. Chem. Phys. **120**, 300 (2004).

[11] E. Schwegler, J. C. Grossman, F. Gygi, and G. Galli, J. Chem. Phys. **121**, 5400 (2004).

[12] V. Dubois, P. Umari, and A. Pasquarello, Chem. Phys. Lett. **390**, 193 (2004).

[13] S. Miertuš, E. Scrocco, and J. Tomasi, Chem. Phys. **55**, 117 (1981).

[14] D. Rinaldi, M. F. Ruiz-Lopez, and J.-L. Rivali, J. Chem. Phys. **78**, 834 (1983).

[15] H. Ågren, C. Medina-Llanos, and K. V. Mikkelsen, Chem. Phys. **115**, 43 (1987).

[16] M. A. Aguilar, F. J. Olivares del Valle, and J. Tomasi, J. Chem. Phys. **98**, 7375 (1993).

[17] A. Klamt and G. Schüürmann, J. Chem. Soc. Perkin Trans. 2, 799 (1993).

[18] J. B. Foresman, T. A. Keith, K. B. Wiberg, J. Snoonian, and M. J. Frisch, J. Phys. Chem. **100**, 16098 (1996).

[19] M. Cossi, V. Barone, R. Cammi, and J. Tomasi, Chem. Phys. Lett. **255**, 327 (1996).

[20] V. Barone and M. Cossi, J. Phys. Chem. A **102**, 1995 (1998).

[21] D. M. York and M. Karplus, J. Phys. Chem. A **103**, 11060 (1999).

[22] M. Cossi, G. Scalmani, N. Rega, and V. Barone, J. Chem. Phys. **117**, 43 (2002).

[23] H. Li and J. H. Jensen, J. Comput. Chem. **25**, 1449 (2004).

[24] R. Car and M. Parrinello, Phys. Rev. Lett. **55**, 2471 (1985).

[25] F. De Angelis, A. Sgamellotti, M. Cossi, N. Rega, and V. Barone, Chem. Phys. Lett. **328**, 302 (2000).

[26] J.-L. Fattebert and F. Gygi, Int. J. Quantum Chem. **93**, 139 (2003).

[27] H. Martin Senn, P. M. Margi, R. Schmid, T. Ziegler, and P. Blöchl, J. Chem. Phys. **118**, 1089 (2003).

[28] S. A. Petrosyan, A. A. Rigos, and T. A. Arias, J. Chem. Phys. *in press.*

[29] J.-L. Fattebert and F. Gygi, J. Comput. Chem. **23**, 662 (2002).

[30] J.-M. Lü, S. V. Rosokha, and J. K. Kochi, J. Am. Chem. Soc. **125**, 12161 (2003).

[31] S. Baroni, A. Dal Corso, S. de Gironcoli, P. Giannozzi, C. Cavazzoni, G. Ballabio, S. Scandolo, G. Chiarotti, P. Focher, A. Pasquarello, K. Laasonen, A. Trave, R. Car, N. Marzari, A. Kokalj, `http://www.quantum-espresso.org/`.

[32] G. Galli and A. Pasquarello. First-principles Molecular Dynamics, in *Computer Simulation in Chemical Physics* (M.P. Allen and D.J. Tildesley Eds., Kluwer Academic Publishers, The Netherlands, 1993).

[33] J. P. Perdew, K. Burke, and M. Ernzerhof, Phys. Rev. Lett. **77**, 3865 (1996).

[34] D. Vanderbilt, Phys. Rev. B **41**, 7892 (1990).

[35] A. Ben-Naim, *Solvation Thermodynamics* (Plenum Press, New York, 1987).

[36] The remaining contributions—thermal energy and $P\Delta V$—are usually negligible and they are rarely considered in continuum approaches.[5]

[37] F. Floris and J. Tomasi, J. Comput. Chem. **10**, 616 (1989).

[38] F. Floris, J. Tomasi, and J. L. Pascual Ahuir, J. Comput. Chem. **12**, 784 (1991).

[39] R. G. Parr and W. Yang, *Density-Functional Theory of Atoms and Molecules* (Oxford University Press, New York, 1989).

[40] H. Reiss, H. L. Frisch, and J. L. Lebowitz, J. Chem. Phys. **31**, 369 (1959).

[41] H. Reiss, H. L. Frisch, E. Helfand, and J. L. Lebowitz, J. Chem. Phys. **32**, 119 (1960).

[42] R. A. Pierotti, Chem. Rev. **76**, 717 (1976).

[43] P. Claverie, in *Intermolecuar Interactions: from Diatomics to Biomolecules* (B. Pullman Ed., J. Wiley, Chichester, 1978).

[44] P. Claverie, J. P. Daudey, J. Langlet, B. Pullman, D. Piazzola, and M. J. Huron, J. Phys. Chem. **82**, 405 (1978).

[45] J. Langlet, P. Claverie, J. Caillet, and A. Pullman, J. Phys. Chem. **92**, 1617 (1988).

[46] M. Heying and D. S. Corti, J. Phys. Chem. B **108**, 19756 (2004).

[47] C. Benzi, M. Cossi, R. Improta, and V. Barone, J. Comput. Chem. **26**, 1096 (2005).

[48] H. H. Uhlig, J. Phys. Chem. **41**, 1215 (1937).

[49] O. Sinanoğlu, J. Chem. Phys. **75**, 463 (1981).

[50] I. Tuñón, E. Silla, and J. L. Pascual-Ahuir, Chem. Phys. Lett. **203**, 289 (1993).

[51] R. C. Tolman, J. Chem. Phys. bf 17, 333 (1949).

[52] F. M. Floris, M. Selmi, A. Tani, and J. Tomasi, J. Chem. Phys. **107**, 6353 (1997).

[53] D. M. Huang, P. L. Geissler, and D. Chandler, J. Phys. Chem. B **105**, 6704 (2001).

[54] M. Cococcioni, F. Mauri, G. Ceder, and N. Marzari, Phys. Rev. Lett. **94**, 145501 (2005).

[55] C. J. Cramer and D. G. Truhlar, J. Am. Chem. Soc. **113**, 8305 (1991).

[56] G. D. Hawkins, C. J. Cramer, and D. G. Truhlar, J. Phys. Chem. B **102**, 3257 (1998), and supporting information.

[57] D. R. Rosseinsky, Chem. Rev. **65**, 467 (1965).

[58] Gaussian 03, Revision B.05, M. J. Frisch et al. Gaussian, Inc., Pittsburgh PA, 2003.

[59] G. Makov and M. C. Payne, Phys. Rev. B **51**, 4014 (1995).

[60] M. Leslie and M. J. Gillan, J. Phys. C: Solid State Phys. **18**, 973 (1985).

[61] G. Spach, H. Monteiro, M. Levy, and M. Szwarc, Trans. Faraday Soc. **58**, 1809 (1962).

[62] R. H. Boyd and W. D. J. Phillips, J. Chem. Phys. **43** 2927 (1965).

[63] O. W. Howarth and G. K. Fraenkel, J. Am. Chem. Soc. **88**, 5414 (1966).

[64] K. Kimura, H. Yamada, and H. Tsubomura, J. Chem. Phys. **48**, 440 (1968).

[65] R. J. Chang, J. Phys. Chem. **74**, 2029 (1970).

[66] M. Itoh, J. Am. Chem. Soc. **92**, 886 (1970).

[67] D. Gundel, H. Sixl, R. M. Metzger, N. E. Heimer, R. H. Harms, H. J. Keller, D. Nöthe, and D. Wehe, J. Chem. Phys. **79**, 3678 (1983).

[68] J. J. Novoa, P. Lafuente, R. E. Del Sesto, and J. S. Miller, Angew. Chem. Int. Ed. **40**, 2540 (2001).

[69] R. E. Del Sesto, J. S. Miller, P. Lafuente, and J. J. Novoa, Chem. Eur. J. **8**, 4894 (2002).

[70] D.-L. Sun, S. V. Rosokha, S. V. Lindeman, and J. K. Kochi, J. Am. Chem. Soc. **125**, 15950 (2003).

[71] D. Small, V. Zaitsev, Y. Jung, S. V. Rosokha, M. Head-Gordon, and J. K. Kochi, J. Am. Chem. Soc. **126**, 13850 (2004).

[72] J. Jakowski and J. Simons, J. Am. Chem. Soc. **125**, 16089 (2003).

[73] DFT deficiencies to represent the binding of neutral van der Waals dimers is well documented. In the case of charged radicals, though, the interactions are of a different nature—essentially electrostatic and covalent—and DFT records good agreement with highly-correlated methods. See D. A. Scherlis and N. Marzari, J. Phys. Chem. B, **108**, 17791 (2004).

[74] J. S. Miller, D. M. O'Hare, A. Charkraborty, and A. J. Epstein, J. Am. Chem. Soc. **111**, 7853 (1989).

[75] H. Bock, K. Ruppert, D. Fenske, and H. Goesmann, Z. Anorg. Allg. Chem. **595**, 275 (1995).

[76] J. S. Miller, J. C. Calabrese, C. Vazques, R. S. McLean, D. T. Glatzhofer, and J. W. Raebiger, Inorg. Chem. **40**, 2578 (2001).

[77] P. Tangney and S. Scandolo, J. Chem. Phys. **116**, 14 (2002).

TABLE I: Solvation and cavitation free energies (kcal/mol) for neutral solutes in water, calculated with this model and with PCM as implemented in Gaussian 03.

	ΔG_{sol}			ΔG_{cav}	
	Expt.[55–57]	This model	PCM	This model	PCM
H_2O	-6.3	-8.4	-5.4	5.7	5.7
NH_3	-4.3	-3.2	-1.6	6.6	6.6
CH_4	2.0	5.4	6.9	7.5	10.0
CH_3OH	-5.1	-3.6	-0.8	9.0	9.6
CH_3COCH_3	-3.9	-1.7	3.5	13.7	14.3
$HOCH_2CH_2OH$	-9.3	-9.3	-6.7	13.0	12.3
CH_3CONH_2	-9.7	-10.5	-4.6	12.7	12.8
$CH_3CH_2CO_2H$	-6.5	-6.0	-2.4	14.8	14.6
mean unsigned error		1.5	4.0		
max. unsigned error		3.4	7.4		

Table P.1

TABLE II: Solvation and cavitation free energies (kcal/mol) for ionic solutes in water, calculated with this model and with PCM as implemented in Gaussian 03.

	ΔG_{sol}			ΔG_{cav}	
	Expt.[55–57]	This model	PCM	This model	PCM
Cl^-	-75	-66.9	-72.6	7.9	5.8
NO_3^-	-65	-57.8	-62.6	10.5	9.7
CN^-	-75	-64.8	-70.2	8.4	7.0
$CHCl_2CO_2^-$	-66	-74.7	-53.5	16.3	15.7
Ag^+	-115	-110.0	-102.3	5.7	4.0
$CH_3NH_3^+$	-73	-81.0	-65.1	9.4	10.2
$CH_3C(OH)CH_3^+$	-64	-70.6	-55.2	13.5	14.4
$C_5H_5NH^+$ (pyridinium)	-58	-60.8	-59.0	15.0	13.9
mean unsigned error		7.1	6.6		
max. unsigned error		9.2	12.7		

Table P.2

Figure Captions:

Figure 1.: Cavity area of a water molecule as a function of Δ (thickness parameter used to evaluate the area, see text) for several values of the electronic density threshold ρ_0.

Figure 2.: Total energy of the NO_3^- anion as a function of the inverse of the lattice parameter, computed in vacuum, in solution, and in vacuum with the Makov-Payne correction up to the leading order.

Figure 3.: Cluster of D_2O molecules used as starting configuration in the molecular dynamics simulations which results are reported in Fig. 4.

Figure 4.: Total and potential energies (top) as a function of time in a molecular dynamics simulation of a cyclic tetramer of heavy water in aqueous solution. The total energy contains the contribution of the Nose-Hoover thermostat. The four curves starting at the bottom of the graph represent the evolution of the intermolecular O$\cdots$H distance between the atoms initially involved in hydrogen bonds.

Figure 5.: Optimized structure of a dimer of $[TCNE]^{-\cdot}$ in dichloromethane, enclosed by an electronic density isosurface at 0.00078 e delimiting the solvation cavity. Carbon atoms in light gray and nitrogen atoms in dark.

Figure 6.: Upper panel: binding energy of two $[TCNE]^{-\cdot}$ anions in dichloromethane as a function of its separation, calculated with only the electrostatic contribution to the solvation energy, and with both the electrostatic and cavitation contributions. Lower panel: area of the solvation cavity as a function of the separation between the $[TCNE]^{-\cdot}$ anions. Above 5 $\mathring{A}$ the cavity splits, and the plotted values correspond to the area of two cavities containing one $[TCNE]^{-\cdot}$ each.

Figure 7.: Time evolution of the intradimer separation (top) and the angle determined by

the central C=C axes of the two monomers (bottom) during a molecular dynamics simulation of $[TCNE]_2^{2-}$ in dichloromethane.

Figure 8.: Characteristic frequencies of the TCNE monomer and dimer extracted from the velocity autocorrelation functions for selected pairs of atoms.

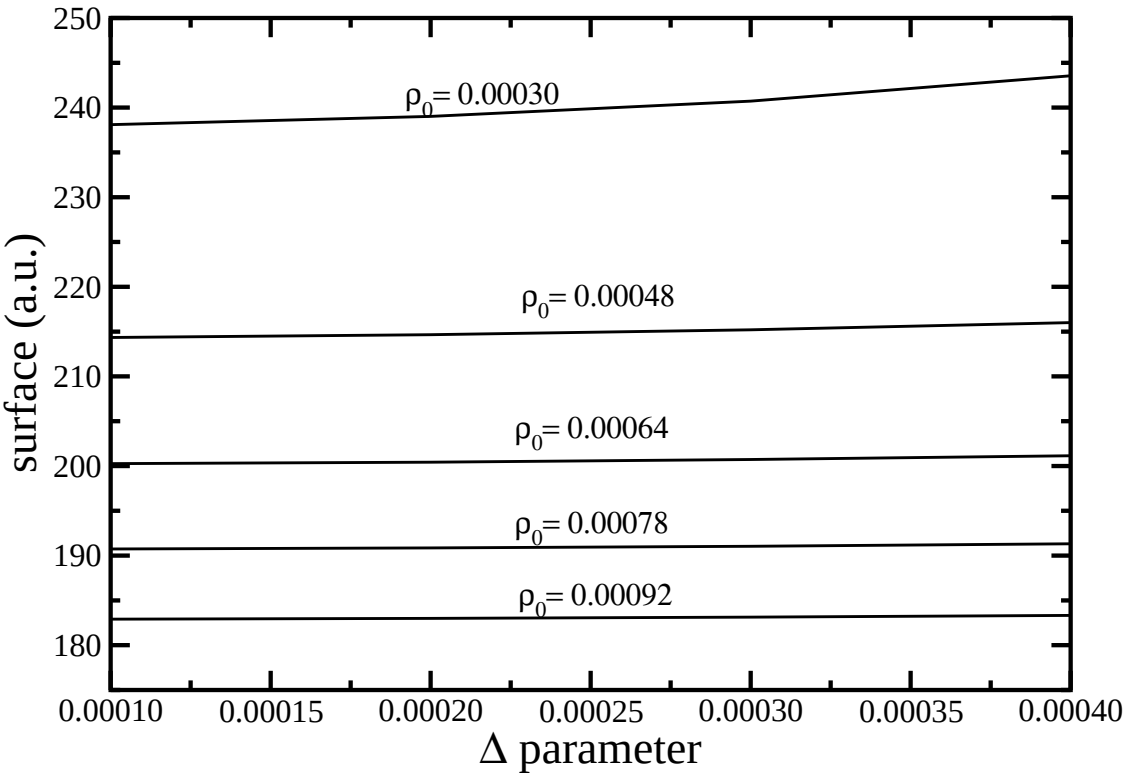

FIG. 1: D. Scherlis

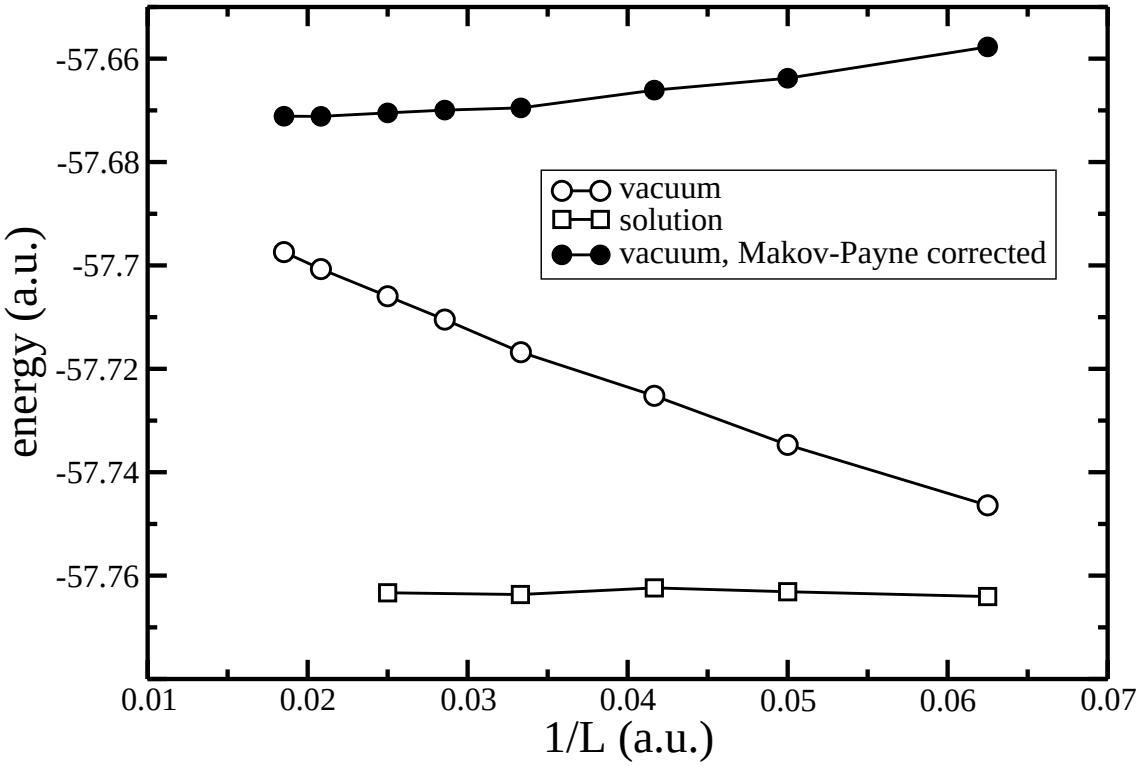

FIG. 2: D. Scherlis

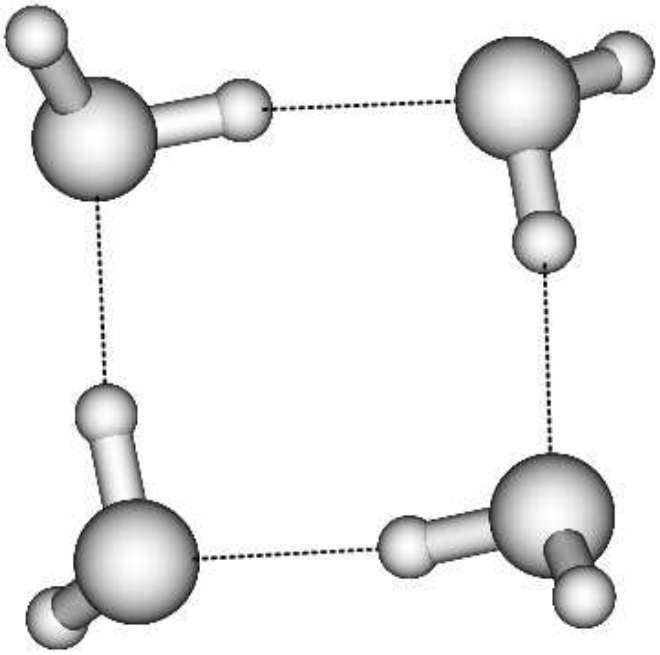

FIG. 3: D. Scherlis

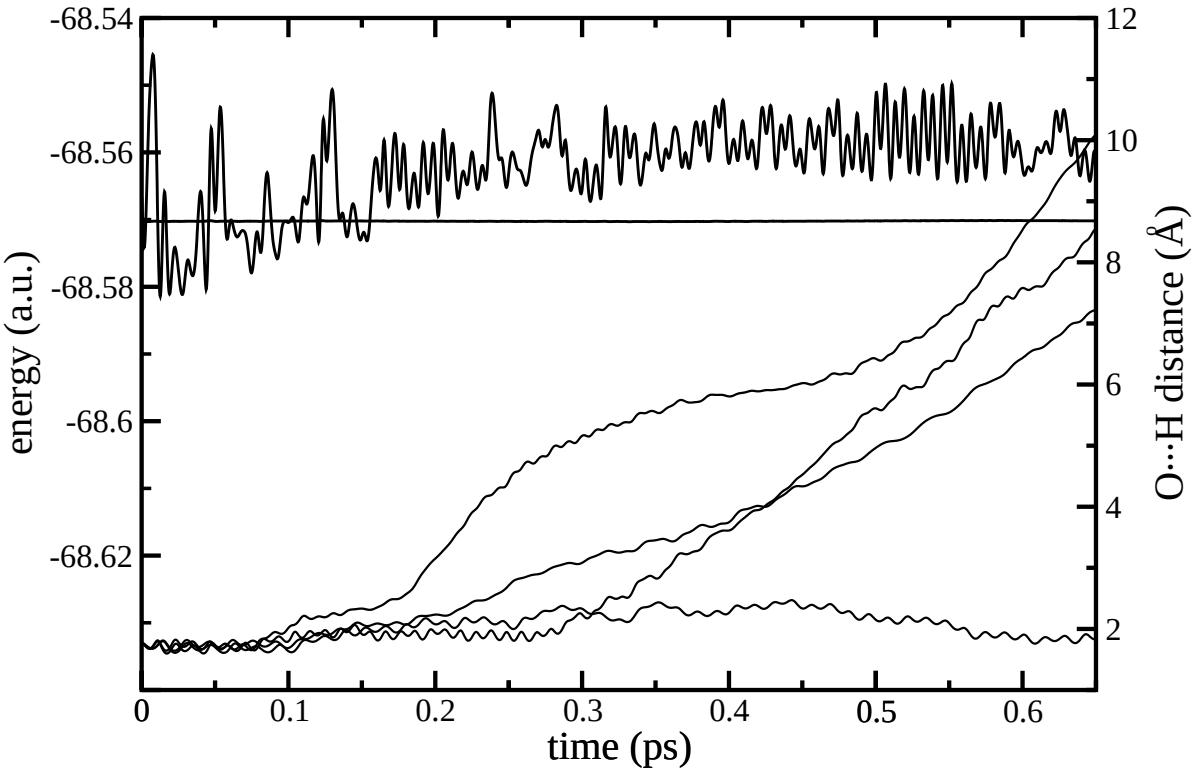

FIG. 4: D. Scherlis

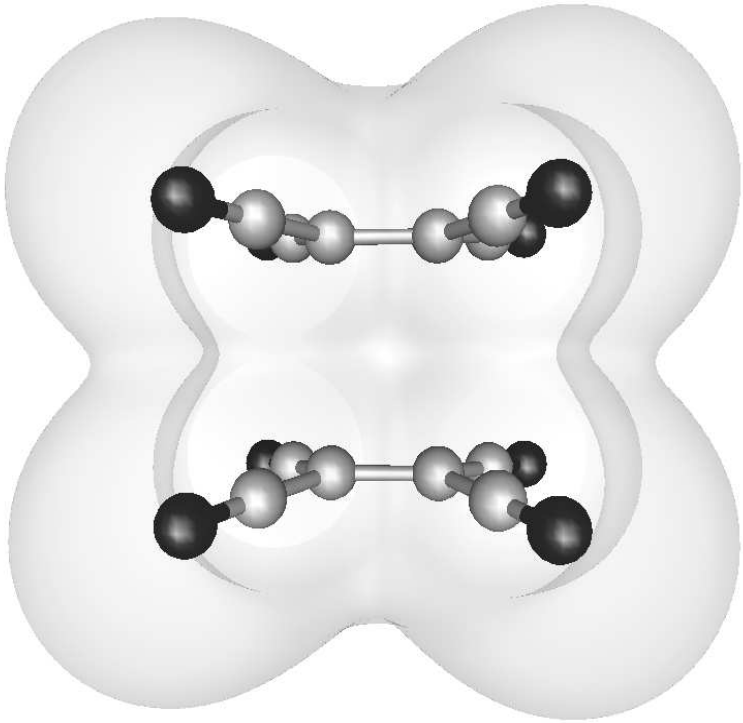

FIG. 5: D. Scherlis

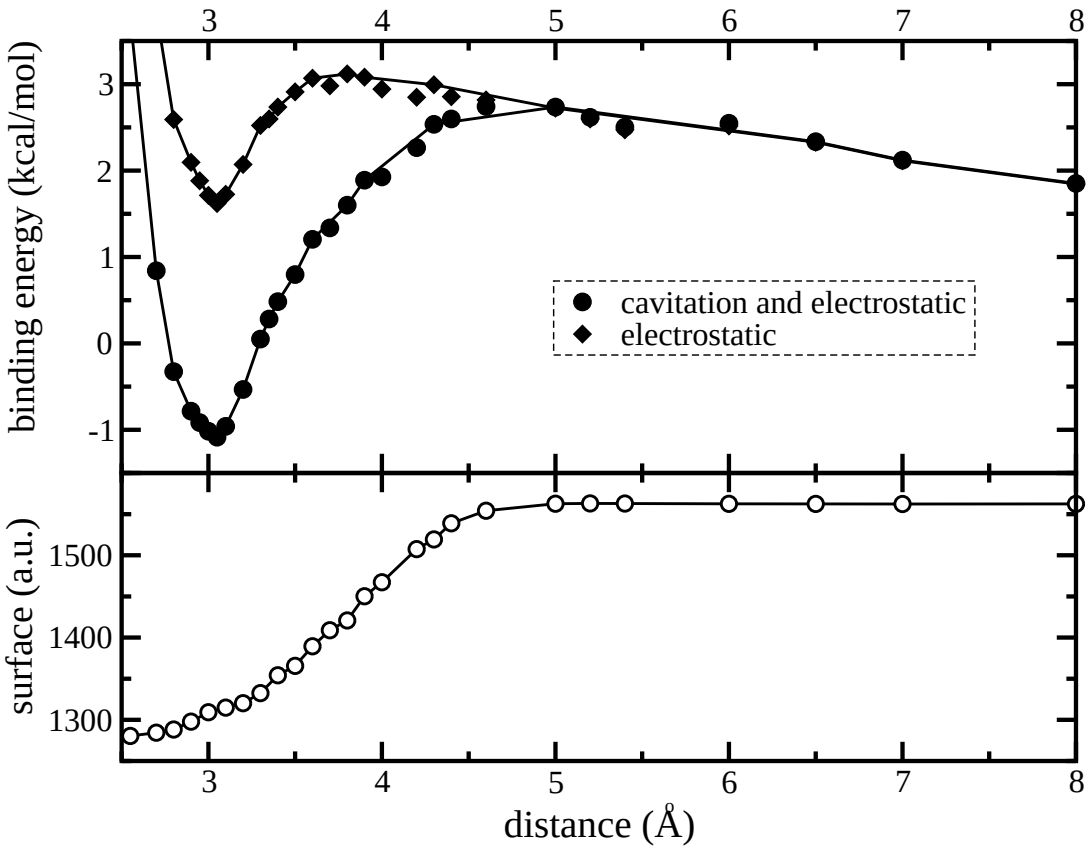

FIG. 6: D. Scherlis

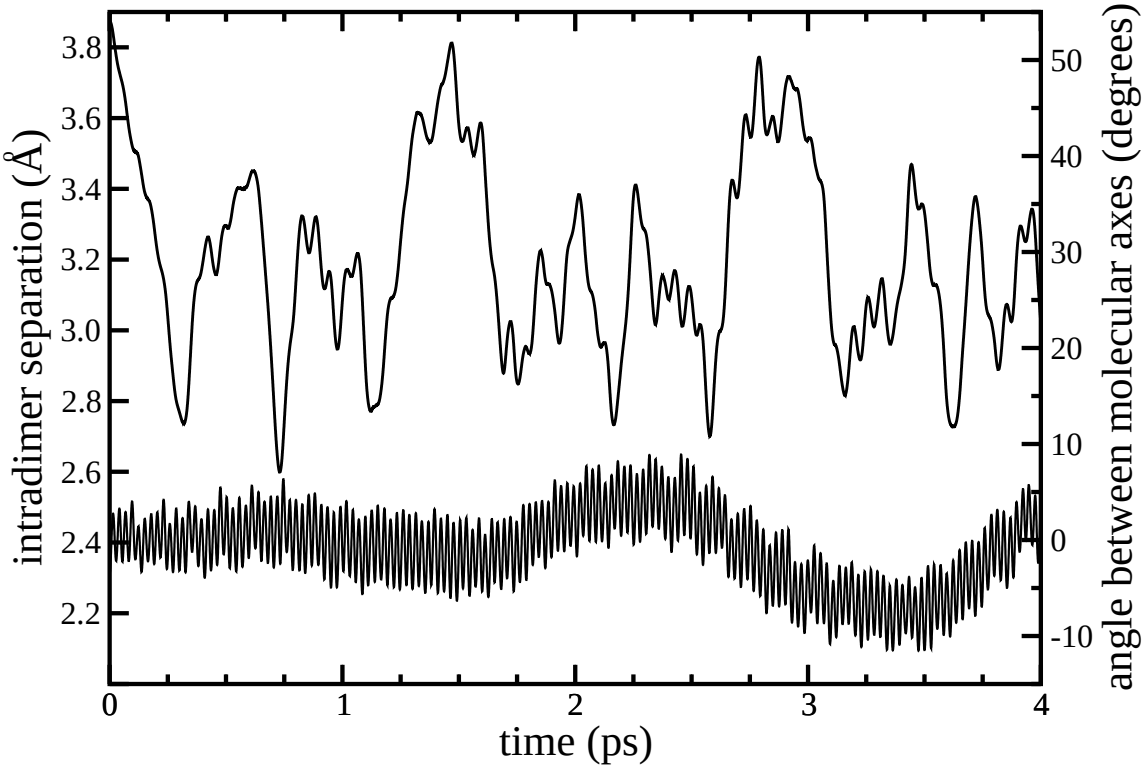

FIG. 7: D. Scherlis

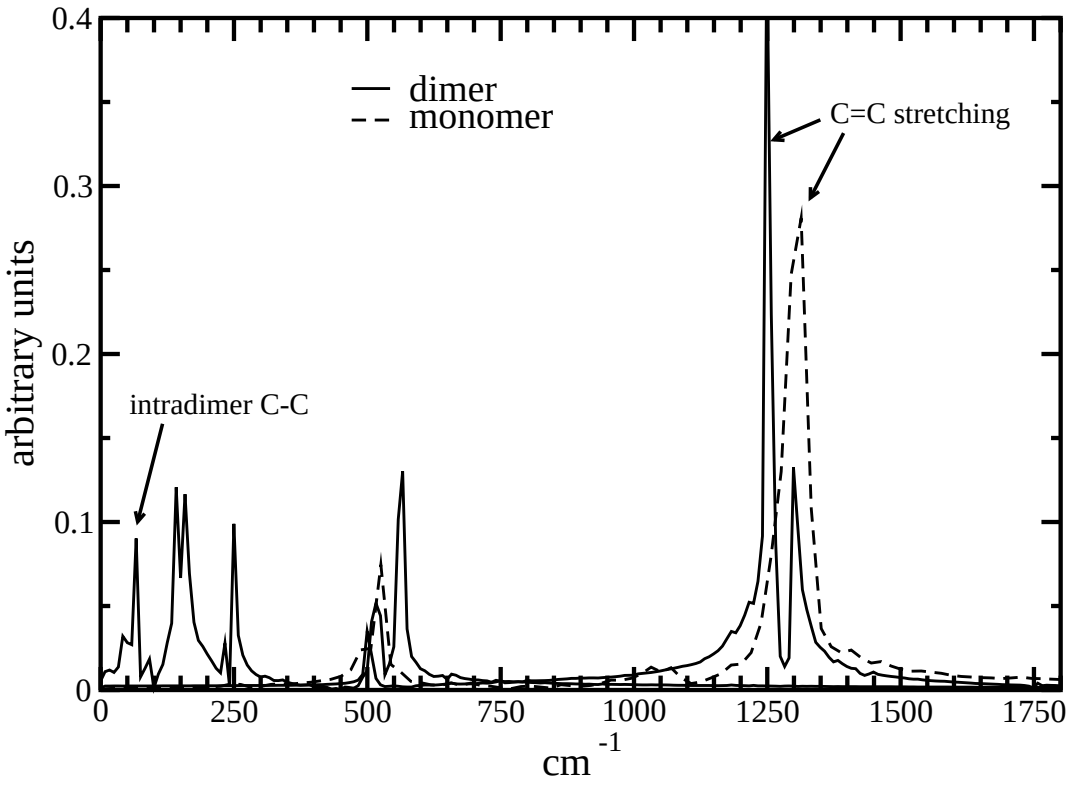

FIG. 8: D. Scherlis